Journal of Engineering Science 15(2), 2024, 79-88
DOI: https://doi.org/10.3329/jes.v15i2.82164

JES
an international Journal

INVESTIGATION OF CRYSTALLITE SIZE, STRAIN EFFECT, INITIAL PERMEABILITY AND OPTICAL PROPERTIES OF Al SUBSTITUTED Ni-Cd DENSE FERRITES

Nur Mohammed[1], Arjumanara Bagum[*1], M. Belal Hossen[1]

[1] *Department of Physics, Chittagong University of Engineering & Technology, Chattogram, Bangladesh*

Received: 18 November 2024 Accepted: 30 December 2024

ABSTRACT

Employing solution combustion technique, Al substituted Ni-Cd nanoparticles were used to prepare bulk specimen, which has the general formula $Ni_{0.65}Cd_{0.35}Fe_{2-x}Al_xO_4$ (x=0, 0.015, 0.030, 0.045, 0.060) and demonstrates how the amount of Al substitution tunes the crystallite size effect, strain effect, permeability and optical properties of the compounds. Crystallite size and strain effect have been investigated using XRD analysis. The formation of a single-phase spinel structure has been confirmed by XRD investigation. The crystallitete size (36 – 39) nm, (36 – 43) nm, (46-64) nm, (38-44) nm and corresponding size strain (2.88×10-3-3.13×10-3), (1.98–3.62), (0.52×10-3-1.07×10-3) and (0.58×10-3-1.31×10-3) have been observed with the help of Scherer's formula, modified Scherer's formula, W-H plot and Strain Size Method respectively. High frequency application has been found in initial permeability study. Cole-Cole plot of initial permeability has been observed narrower semicircles with increasing Al content. UV-vis spectroscopy has been used to study optical properties and observed that with increasing Al content reflectance decreases in the (400-700) nm wavelength range. Band gap energy has been found in the range of 1.62 eV to 1.68 eV

Keywords: *Nanocrystalline powder; XRD; Optical properties; initial permeability*

1. INTRODUCTION

The soft magnetic compound known as ferrite materials which are a combination with mixed oxide of iron and one or more other metals having ferrimagnetic characteristics (Abdul Mannan & Belal Hossen, 2021). A substantial amount of iron oxide (Fe_2O_3) combined with minute amounts of metallic metals like Zinc (Zn), Cadmium (Cd), Cobalt (Co), Nickel (Ni), and Manganese (Mn) in ferrites. Ferrites are distinguished as soft ferrites and hard ferrites. While hard ferrites, because of their higher H_c and M_r, are more difficult to magnetize and demagnetize, soft ferrites have the capacity to do so (Munir et al., 2022). Ferrimagnetic materials with spinel structure are thought to be very advantageous for optical and magnetic applications. Soft spinel ferrites are ceramic magnetic materials with substantial technical applications that are widely employed in a variety of fields (Ponpandian & Narayanasamy, 2002). Spinel ferrites are a strong contender for many applications due to their excellent magnetic, electrical, and microwave properties (Hasan & Azhdar, 2022), magnetic read-write head cores for fast digital tape or disk recording (Hossen & Hossain, 2015), microwave absorbers and magnetostrictive (Munir et al., 2022), MRI, thermotherapy and biotechnological applications, satellite communication, transformers, memory storage device (Yadav et al., 2019). Many electronic applications require high density solids instead of nanoparticles (Valenzuela et al., 2016). A spinel structure known as crystallite is formed by the combination of tetrahedral (8A) sites and Octahedral (16B) sites occupied by cations only out of available 64 A sites and 32 B sites. A spinel ferrite's unit cell is made up of 32 oxygen atoms, 8 divalent metal ions (M), and 16 trivalent ions. Two interstitial spaces in the spinel structure are occupied by metal cations with oxygen coordination on their B and A sites atoms (Massoudi et al., 2020; Rahman et al., 2022). Which magnetic ions are present on the A and B sites, as well as the relative concentration of the inter (J_{AB}) and intra-sublattice (J_{AA}, J_{BB}) exchange contracts, control the magnetic characteristics of spinel ferrites (Nath et al., 2012). Typically, Ni prefers to occupy the B sites while Cd follows to occupy the A site, in the case of Ni-Cd mixed ferrite materials. While Cd ferrite has a typical normal spinel structure, and Ni ferrite belongs to inverse spinel structure (Chau et al.2008). Combined the structure of Ni-Cd ferrites is mixed spinel ferrite. Cd^{2+} and Fe^{3+} are found at the A sites, while Ni^{2+} and Fe^{3+} are found at the B sites.

As an alternative of Ni-Zn ferrites Ni-Cd have superior , magnetic and optical properties can change as a result of the interactions between the ions in their A and B locations (Reddy, 2021). Successful fabrication of ferrites containing nickel (Ni) and extensive characterization of those ferrites have been accomplished, because of their enormous multifunctional applications due to their comparably higher inductive property at higher frequency

*Corresponding Author: *arjumancuetphy@gmail.com*

ISSN 2075-4914 (print); ISSN 2706-6835 (online)

regions, reasonably low demagnetizing as well as dielectric losses, and obviously lower electrical conductivity (Abdul Mannan & Belal Hossen, 2021). In mixed ferrites, Cd-ferrite is significant because of its high resistivity, high permeability, and relatively low magnetic losses (Batoo et al., 2009). Making multilayer ferrite chip components is crucial for the downsizing of several devices in the fields of electronic device and energy storage appliances (Hossen & Hossain, 2015; Munir et al., 2022).

Substitution of stoichiometric trivalent ions in the present spinel materials perform an important function to obtain materials with unique physical properties as well as improved electrical and magnetic properties (Shahzadi et al., 2020). Spinel ferrites have been shown to enhance optical and magnetic characteristics due to the preference of tightly doped non-magnetic (Al^{3+}) ions for Fe^{3+} and studies have provided helpful information on the type of exchange contact, the magnetization direction, the distribution of the cations, the spin canting, etc. (Batoo et al., 2009). Particle size is getting close to the critical size, below which each particle is treated as a single domain, the characteristics of bulk ferrites using nano particles are significantly impacted. Magnetic and dielectric properties of ferrite are significantly influenced by the order of conductivity in grain boundaries. Interesting magnetic features including spin canting and uniform domain size improve characteristics of bulk specimen using nano powders. The grain boundaries govern the physical properties than grains (Reddy, 2021).

Due to their low coercivity, remanence, and moderate saturation magnetization values, Ni-Cd ferrites and also Al substituted Ni-Cd ferrites offers interest to scientific community (Abdul Mannan & Belal Hossen, 2021; Mahmood & Hossen, 2021). Many scientists have looked into Al substituted Ni-Cd ferrites. Al substituted Ni-Cd ferrite raises the optical, magnetic, resistivity and lowers the dielectric losses. Al substitution also modifies the structural and optical characteristics of materials (Batoo, 2011; Şaşmaz Kuru et al., 2018). $Ni_{0.20}Cd_{0.30}Fe_{2.5-x}Al_xO_4$ have been looked for and reported single phase spinel cubic structure (Batoo et al., 2009). They have been determined grain size (3-7) nm using Scherrer's formula. $Ni_{0.5}Cu_{0.2}Cd_{0.3}Fe_{2-z}Al_zO_4$ with step 0.015 ferrite nanoparticles have been fabricated by (Abdul Mannan & Belal Hossen, 2021) and showed single phase spinel structure with Al substitution. X-ray Analysis of $NiFe_2O_4$ nanoparticles by Williamson-Hall and Size-Strain Plot Method has been observed (Sapna et al., 2018) and they determined 34.9 nm, 27.4 nm and 23.5 nm by Scherrer method, Williamson-Hall plot and size strain plot. Band gap energy (3.16 -4.5) eV has been observed by (Massoudi et al., 2020) in Magnetic and spectroscopic properties of Ni–Zn– Al ferrite spinel: from the nanoscale to microscale. These ferrites were recently synthesized using a variety of processes to obtain narrow size distributed microstructure, which improved their physical properties and expanded the range of applications for them (Ponpandian & Narayanasamy, 2002). Sol-gel technology has been utilized to produce products with small, homogeneous particles, chemical homogeneity, high purity, and low energy savings. For Ni-Cd ferrites, microscopic features like composition, grain size, dopant quantity, impurities, production process, and heating conditions are important (Hasan & Azhdar, 2022).

The aforementioned research indicate that more attention needs to be paid to the Al substitution effect on Ni-Cd ferrites in various fields, particularly to their structural, electric, and magnetic properties. In order to study the size effect, size strain effect, magnetic and optical properties, $Ni_{0.65}Cd_{0.35}Fe_{2-x}Al_xO_4$ has been chosen in present research due to its unique features. Many curious minds are keeping an eye out to look at the changes in characteristics as a result of this fact even though very few structures have been reported on the effect of Al addition up to this point. In light of that perspective, we have been focused on Al substituted Ni-Cd bulk ferrite obtained from nanocrystalline powder.

2. MATERIALS AND METHODS

To synthesize of $Ni_{0.65}Cd_{0.35}Fe_{2-x}Al_xO4$ (NCA) the necessary ingredients have been used $Ni(NO_3)_2.6H_2O$(99%), $Cd(NO_3)_2.4H_2O$(98%) , $Al(NO_3)_2.9H_2O$(99.5%) and $Fe(NO_3)_2.9H_2O$ (98%). A series of $Ni_{0.65}Cd_{0.35}Fe_{2-x}Al_xO4$ with step 0.015, nanoparticles have been fabricated using the sol-gel auto-combusted method and with the addition of pure ethanol solution. In the necessary ethanol solution, the stoichiometric mixture of substances has dissolved. Liquid ammonia (25%) has been used to keep the solution's pH at 7. A magnetic stirrer is used to swirl the above solution constantly while keeping the temperature at 80 °C until a gel form. The resulting gel was heated for five hours at 250 °C. As the gel heats up, it starts to ignite itself. Heating has caused the entire gel to flame out, forming a loose, fluffy powder. To form the single-stage NCF ferrite nanopowders, the resulting powder has been annealed for five hours at 700 ºC. Using nanopowders and PVA as binders, disc and toroid-shaped specimens were created. The disc and ring-shaped samples are then sintered at 1150 ºC to densify them for the required specimen properties. The schematic diagram of the synthesis process is presented in Fig 1.

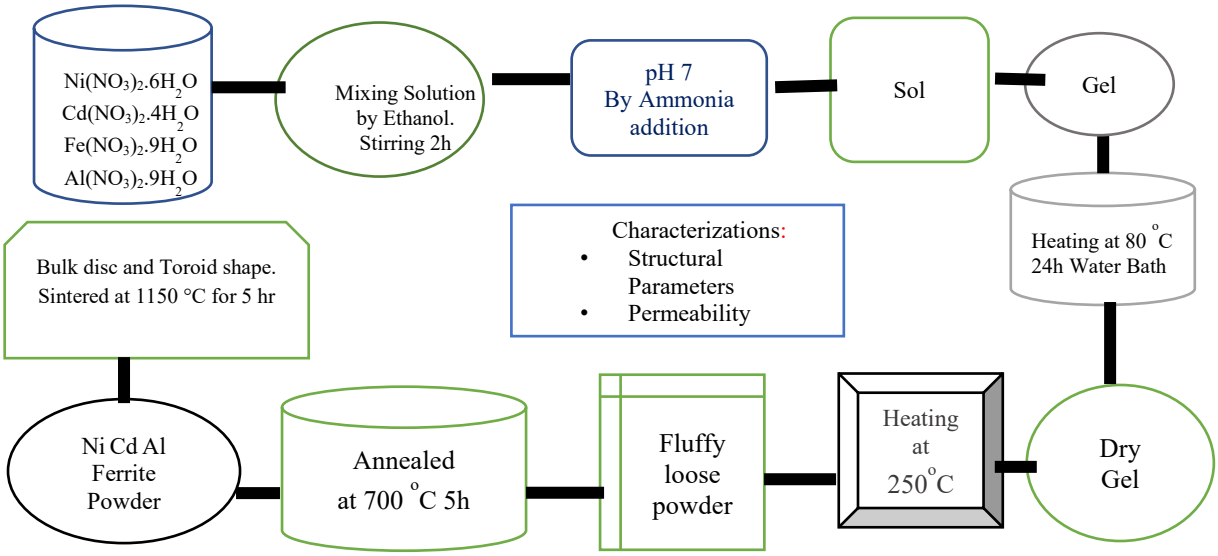

Figure 1: Flow chart for sol-gel process of $Ni_{0.65}\,Cd_{0.35}\,Fe_{2-x}\,Al_xO_4$.

The Scherrer's formula D = (Kλ/ βcosθ) has been used to calculate the crystallite size, where D is crystallite size, β signifies for the whole width half maximum, θ represents for the crystal's diffraction angle, λ indicates for the wavelength of the Cu-Kα compound (1.5405 Å), and k symbolizes for the form factor (0.9). When compared to the Scherrer approach, the W-H analysis is a more straightforward integral breadth method that fluctuates with tan θ rather than following a 1/cosθ dependency. The analysis described below predicated on the notion that the diffraction line broadening brought on by crystallite size (D) and crystal micro strain (S) are values that add up $\beta_{hkl} = \beta_D+\beta_s$. Line broadening of the diffraction peak caused by the microstrain is given by $\beta s = 4\varepsilon\tan\theta$ (Kulkarni & Mathad, 2018) . So, the W-H equation can be expressed as $\beta_{hkl}\cos\theta = (k\lambda/D) +4\varepsilon\sin\theta$. The uniform deformation model (UDM), which claimed that the strain equal in all crystallographic directions. According to the W-H plot, line broadening is an isotropic phenomenon.

However, a better assessment can be made by considering the average size strain plot, which places less emphasis on data from higher angles where accuracy is typically lower. For the sake of this approximation, it has assumed that "strain" and "crystallite size" are represented by Gaussian and Lorentzian functions, respectively. Similar to this, we obtain: $(d_{hkl}\beta_{hkl}\cos\theta)^2 = k\lambda/D(d_{hkl}^2\,\beta_{hkl}\cos\theta) +(\varepsilon/2)^2$, where d_{hkl} denotes the lattice spacing and k denotes constant which depend on the particle's formation (Sapna et al., 2018). Kubelka-Munk theory $F(R) = (1 - R)^2/2R$ has been used to estimate the optical absorption coefficient (α) by analyzing reflectance data, where F(R) denotes Kubelkae-Munk function and R symbolize reflectance (Jogi et al., 2022). The following is how the complicated permeability dispersion of frequency is stated, $\mu_i^*=\mu_i' + \mu_i''$, where μ′ represents the magnetic induction component for energy that is consumed and μ″ represents the alternating magnetic field component for energy loss. Following relation can be used to compute the real and imaginary portion of initial permeability $\mu_i' = L_s/L_o$ and $\mu_i'' = \mu_i'\tan\delta$, where L_s stands for the self-inductance of the sample core, $L_o = (\mu_o N^2 h/ 2\pi)\ln(R_2/R_1)$, Here, N stands for number of turns of coil, h stands of thickness and R_2 and R_1 stands mean outer and inner radius of toroid shape sample (Alam et al., 2014; Hossen & Hossain, 2015).

3. RESULTS AND DISCUSSION

3.1 STRUCTURAL WITH SIZE AND STRAIN ANALYSIS

An X-ray diffractometer has been used to examine the structural with size and strain characteristics of Al substituted NCF bulk spinel ferrite (NCA) $Ni_{0.65}\,Cd_{0.35}\,Fe_{2-x}\,Al_xO_4$ with steps x = 0.015. Cu-Kα radiation (λ = 1.5405 Å) has been used to obtain the XRD pattern for each composition at room temperature in 2θ range of 10° to 70°. It has observed that, the diffraction patterns shown the development of cubic spinel structure with space

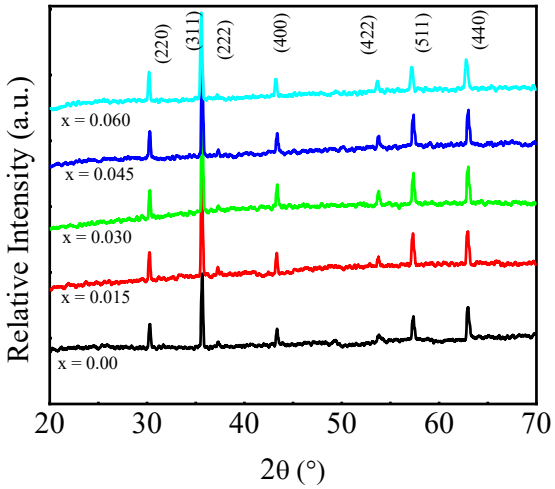

Figure 1: X-ray diffraction pattern of $Ni_{0.65}Cd_{0.35}Fe_{2-x}Al_xO_4$.

group Fd3m. XRD image (Fig. 2) shown that a single-phase cubic spinel structure has successfully been formed and that no secondary peaks have observed. The identified diffraction planes are (220), (311), (222), (400) (422), and (511) and (440). (Birajdar et al., 2012; Nath et al., 2012; Rahman et al., 2022). The most intense diffraction peak plane (311) has been identified that how material grew preferentially along that plane. The Scherrer's formula has used to estimate the crystallite size of compound which found to be between 36 to 39 nm with a high intense peak corresponding to the (311) plane. Table 1 has been provided a summary of structural size and strain contents of compounds.

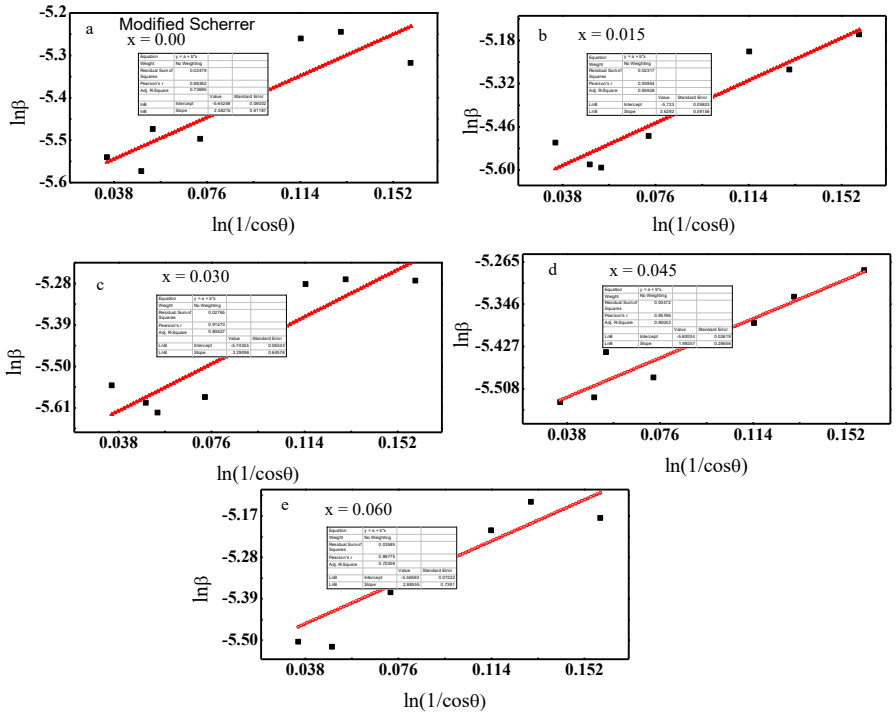

Figure 2: Crystallite size determination of $Ni_{0.65}Cd_{0.35}Fe_{2-x}Al_xO_4$ by modified Scherrer's approach for (a) x = 0, (b) x= 0.015, (c) x= 0.030, (d) = 0.045 and (e) = 0.060.

Fig.1 has been depicted about the modified Scherrer's formula to estimate the size of which found from (36-43) nm with the same (311) plane recorded in Table 1 (Sapna et al., 2018). It is possible to draw a straight line with an intercept equal to ln (kλ/D) by plotting between lnβ and ln(1/cosθ) from modified Scherrer approach which was given crystallite size.

Fig. 3 has been illustrated about the Williamson-Hall (W-H) formula to measure the crystallite size which have found from (46-60) nm shown in Table 1. When compared to the Scherrer approach, the W-H analysis is a more straightforward integral breadth method that fluctuates with $\tan\theta$ rather than following $1/\cos\theta$ dependency. The uniform deformation model asserted that strain is equal in all crystallographic orientations. The term $(4\sin\theta)$ has been used to plot the term $(\beta_{hkl}\cos\theta)$ in Fig. 3.

The strain and crystallite size have been determined by the fitted line's slope and vertical axes Y-intercept, respectively in Fig.4 (Hasan & Azhdar, 2022; Kulkarni & Mathad, 2018; Shetty et al., 2023) . The W-H analysis has been shown in Table 1. Fig. 5 has been demonstrated about the Size Strain Method (SSM) to measure the crystallite size of NCF found from (38-44) nm. The term $(d_{hkl}\beta_{hkl}\cos\theta)^2$ has plotted against the $(d_{hkl}{}^2\ \beta_{hkl}\cos\theta)$. Crystallite sizes have been derived from the slope of the linearly fitted data from size strain method shown in Table 1 .The Scherrer equation only takes into consideration significant peaks, whereas both the W-H approach and the SSM plot, which also take into account the strain rectification component, result in further reductions in crystallite size (Sapna et al., 2018).

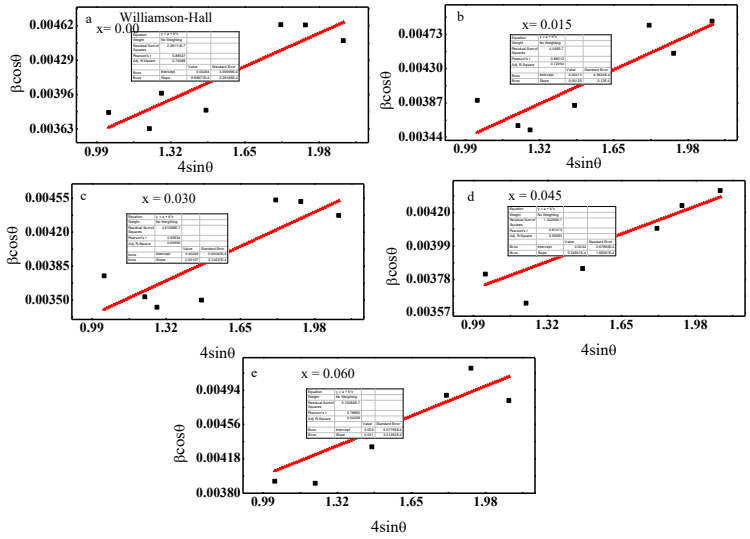

Figure 3: Crystallite size determination of $Ni_{0.65}Cd_{0.35}Fe_{2-x}Al_xO_4$ by Williamson-Hall Method for (a) x = 0, (b) x= 0.015, (c) x= 0.030, (d) = 0.045 and (e) = 0.060.

Table 1: The crystallite size (D) and strain (ε) using, The Scherrer's formula, W-H plot and Size-Strain Plot.

Al contents	The modified Scherrer's formula		Williamson-Hall method		Size-strain plot	
	D (nm)	ε ($\times10^{-3}$)	D (nm)	ε ($\times10^{-3}$)	D (nm)	ε ($\times10^{-3}$)
0	38	2.95	46	0.70	40	1.07
0.015	39	2.92	64	1.29	44	1.31
0.030	39	2.88	60	1.07	42	0.97
0.045	37	3.09	43	0.52	38	0.58
0.060	36	3.13	46	1.00	38	1.59

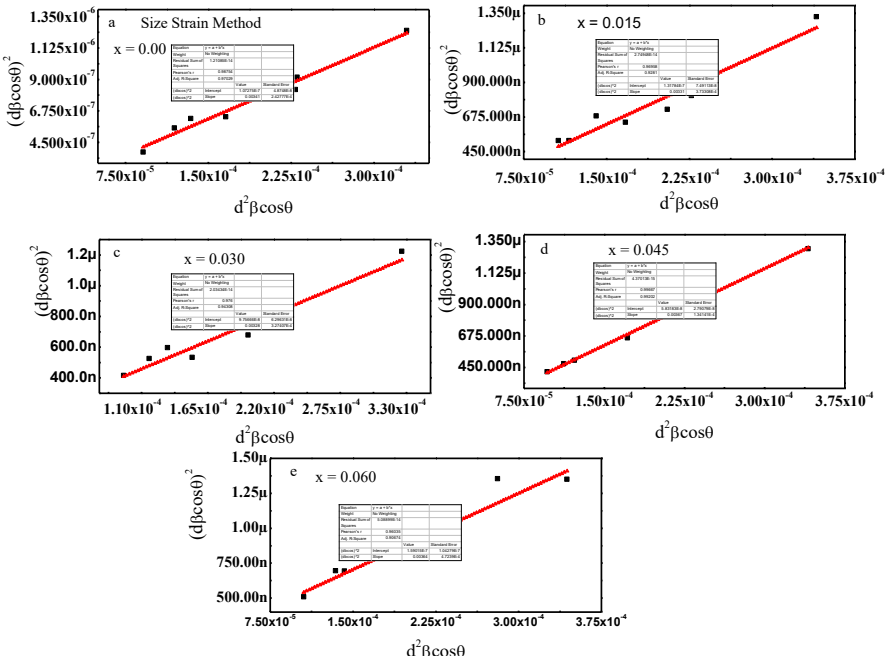

Figure 4: Crystallite size determination of $Ni_{0.65}Cd_{0.35}Fe_{2-x}Al_xO_4$ by SSM for (a) x = 0, (b) x= 0.015, (c) x= 0.030, (d) = 0.045 and (e) = 0.060.

The Scherrer's equation has been taken only consideration significant peaks, whereas both the W-H approach and the size-strain plot method, which also take into account the strain rectification component, result in further reductions in crystallite size (Sapna et al., 2018). By using W-H plot method crystallite size have found from 46 nm to 64 nm, whereas size-strain plot method 38 nm to 44 nm.The substitution of Al within a material can disrupt the arrangement of the crystal lattice, which may lead to a smaller size of the crystallites.Higher levels of Al substitution are associated with a decrease in crystallite size, which is accompanied by an increase in lattice strain (Zak et al., 2024).

3.2 COMPLEX INITIAL PERMEABILITY STUDIES

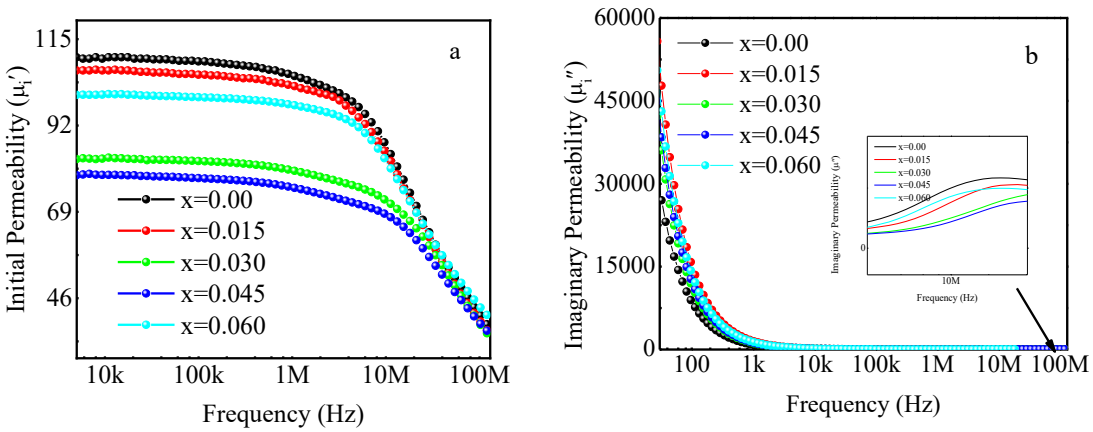

Figure 5: Demonstrates (a) the μ_i' and (b) μ_i'' of the initial permeability as based on the frequency.

Fig. 5a and 5b have been displayed the μ_i' and μ_i'' of compound with frequency. Up to 8MHz frequency, the μ_i' is pretty steady, but beyond that, it alters and then quickly decreases with Al content and frequency. The substitution of Al for Fe in a ferrite changes the distribution of cations and induces structural changes, which in turn affect the configuration of magnetic domains and the movement of domain walls (Zakaria et al.,2009).

The μ_i' parameter used to express the in phase relationship between the magnetic induction component (B) and the alternating magnetic field (H), assesses the capacity of materials to store energy, while the μ_i'' parameter measures the ability of materials to dissipate energy.

In contrast, the μ_i'' rapidly declines at lower frequency sides and has a typical peak at higher frequency sides, where the μ_i' begins to decline. It's known as the ferrimagnetic resonance phenomena (Ali et al., 2019). The two separate magnetization mechanisms such as domain wall motion and spin rotation are related to the permeability of spinel ferrites. In comparison to spin rotation, domain wall motion contributes more to permeability at lower frequencies. Large grains facilitate domain wall motion, resulting in high permeability. The domain's wall causes the initial permeability to be represented as, $(\mu_i')_w = (3\pi M_s^2 D_m)/4\gamma$, $(\mu_i')_{spin} = (2\pi M_s^2)/k$, where M_s stands for saturation magnetization, D_m stands for average grain size, K for the magnetocrystalline structure's anisotropy constant and γ for domain wall energy (Islam et al., 2019). The particle size, saturation magnetization, and magnetocrystalline anisotropy influence the initial permeability (Birajdar et al., 2012). Variation of initial permeability can be made in a number of ways, including high density structures, saturation magnetization thin grain boundaries with large grain sizes, and chemical composition optimization (Mostafa et al., 2022).

3.3 Cole-Cole of Complex Initial Permeability Studies

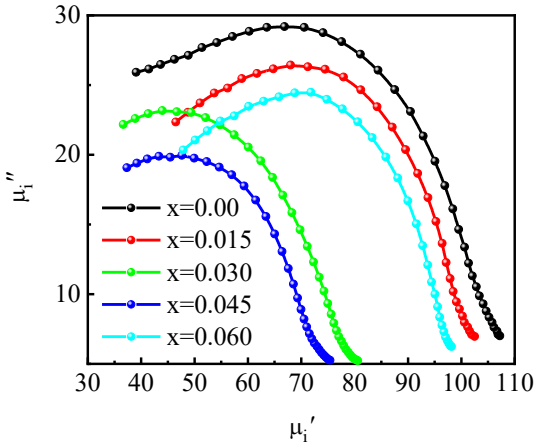

Figure 6: Cole–Cole plots for $Ni_{0.65}Cd_{0.35}Fe_{2-x}Al_xO$.

The Cole–Cole plot for the curves of μ_i* is presented in Fig. 6. The semicircle-shaped curves in this plot of μ_i''-μ_i' indicate the relaxation dispersion (Smit et al., 1959). In a variety of applications, the Ni-Cd-Al ferrites and other spinel ferrites exhibit relaxation phenomena as frequency increases because of the attenuation of the magnetization process. The Cole–Cole plot also describes the relation between the magnitude of μ_i* and relaxation of the compounds. The peak width of the μ_i''-μ_i' curves narrows as the Al content rises rises indicating a reduction in the distribution of relaxation times with Al substitution (Jelonek et al., 1978), and a significant shift in the maximum of μ_i'' at higher frequencies is observed. As demonstrated by Fig. 6, the f_{res} of Ni-Cd-Al ferrites rises above that of pure Ni-Cd ferrites. Domain wall stabilization is responsible for this enhancement, which lowers high frequency losses (Nam et al., 1995).

3.4 QUALITY FACTOR

Fig. 7 has been shown the quality factor (Q-factor) fluctuations of the compound. The Al substituted compound has been shown wider peak widths than the parent compound. These wider peak widths offer a broad brand frequency as well as Q-factor value shift towards higher frequency side implies application range suitable for that more accurate method of assessing magnetic characteristics. A favorable peak in the Q-factor for samples containing Al occurs at a frequency of about 1 MHz. Higher Q-factor has observed for x = 0.060 in the middle region of frequency.

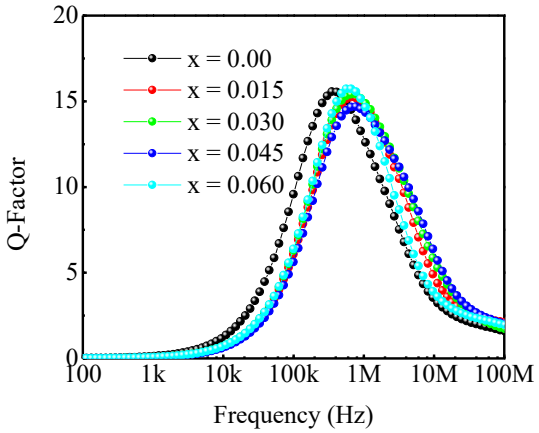

Figure 7: Q-factor versus frequency of NCF.

3.5 OPTICAL PROPERTIES

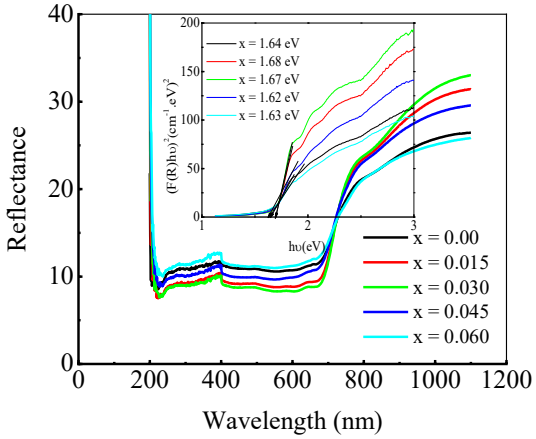

Figure 8: Band gap measurement of Ni-Cd-Al ceramics spinel ferrite using Kubelka-Munk theory.

Fig. 8 has been illustrated that the band gap energy estimation of materials using this reflectance data (Jogi et al., 2022). UV-vis spectroscopy has been used to record reflectance data between 200 nm and 1200 nm at room temperature. In order to comprehend the optical characteristics of $Ni_{0.65}Cd_{0.35}Fe_{2-x}Al_xO_4$, UV-visible absorption spectra have used. All samples having their UV-visible absorbance spectra have recorded between 200 and 800 nm at room temperature. It has been revealed that Ni-Cd-Al spinel bulk ferrite exhibits strong UV and visible light reflectance. By extrapolating the linear section of the plot $(\alpha h\nu)^2$ versus hν to zero absorption making intercept at energy axis, the optical band gap (E_g) have been calculated from 1.64 eV, 1.68 eV, 1.67eV, 1.62 eV and 1.63 eV of compound as direct band gap transition (Sattar et al., 2022). For various ferrite compounds, it has been reported that a similar result by (Sharma et al., 2021).

4. CONCLUSIONS

NCF bulk ferrite compound has been successfully synthesized using the sol-gel auto-combustion method to fabricate dense specimen. Investigation have been made on the basis XRD data which explores the structural with crystallite size as well as strain effect. The single-phase homogenous cubic spinel structure of every compositions has been revealed by XRD analysis. Optical properties of the NCF spinel ferrite have been explored as semiconductor nature. Modified Scherer's formula, the W-H plot, and the strain size method have been used to determine the crystalline size, which to be 36–39 nm, 43–64 nm, and 38–42 nm and corresponding size strain. According to UV-Vis research, the band gap energy has been found from 1.62 eV to 1.68 eV. High frequency application has been confirmed by permeability studies.

ACKNOWLEDGEMENT

The authors acknowledge the sample preparation help taken from Department of Physics, Chittagong University of Engineering and Technology, Chattogram, Bangladesh.

REFERENCES

Abdul Mannan, M., & Belal Hossen, M. (2021). Dynamic electric, modulus and impedance study of $Ni_{0.5}Cu_{0.2}Cd_{0.3}Fe_{2-z}Al_zO_4$ nanoparticles with magnetization and Rietveld analysis. *J. Mater. Sci.: Mater*, 32(19), 24524–24539. https://doi.org/10.1007/s10854-021-06930-2

Munir, M. A., Naz, M. Y., Shukrullah, S., Ansar, M. T., Farooq, M. U., Irfan, M., Nasar, S., Mursal, F., Legutko, S., & Petr, J. (2022). Enhancement of Magnetic and Dielectric Properties of $Ni_{0.25}Cu_{0.25}Zn_{0.50}Fe_2O_4$ Magnetic Nanoparticles through Non-Thermal Microwave Plasma Treatment for High-Frequency and Energy Storage Applications, *Materials* **2022**, *15*(19), 6890; https://doi.org/10.3390/ma15196890.

Hossen, M. B., & Hossain, A. K. M. A. (2015). Structural and dynamic electromagnetic properties of $Ni_{0.27}Cu_{0.10}Zn_{0.63}Al_xFe_{2-x}O_4$. *J. Magn. Magn. Mater.*, 387, 24–36. https://doi.org/10.1016/j.jmmm.2015.03.083

Hasan, S., & Azhdar, B. (2022). Synthesis of Nickel-Zinc Ferrite Nanoparticles by the Sol-Gel Auto-Combustion Method: Study of Crystal Structural, Cation Distribution, and Magnetic Properties. *Adv. condens. matter phys.* , 2022:1-14 2022. https://doi.org/10.1155/2022/4603855

Yadav, A., Choudhary, P., Saxena, P., Rai, V. N., & Mishra, A. (2019). Spectroscopic analysis and temperature-dependent dielectric properties of bulk Ni-Zn ceramics. *J. Adv. Dielectr.*, 9(2), 1–12. https://doi.org/10.1142/S2010135X19500140

Valenzuela, R., Gaudisson, T., & Ammar, S. (2016). Severe reduction of Ni-Zn ferrites during consolidation by Spark Plasma Sintering (SPS), *J. Magn. Magn. Mater.*, 400, 311–314. https://doi.org/10.1016/j.jmmm.2015.07.044

Nath, S. K., Maria, K. H., Noor, S., Sikder, S. S., Hoque, S. M., & Hakim, M. A. (2012). Magnetic ordering in NiCd ferrite. *J. Magn. Magn. Mater.*, 324(13), 2116–2120. https://doi.org/10.1016/j.jmmm.2012.02.023

Chau N. , Thuan N.K , Minh D.L , Luong N.H. (2008). Effects of Zn content on the magnetic and magnetocaloric properties of Ni-Zn ferrites,VNU *J. Sci. Math. Phy.* 24, 155.

Reddy, N. V. (2021). Structural and Magnetic Properties of Al^{3+} Doped NI-ZN Nano Ferrites. *IARJSET*, 8(6), 313–316. https://doi.org/10.17148/IARJSET.2021.8654

Shahzadi, K., Chandio, A. D., Mustafa, G., Khalid, M., Khan, J. K., Akhtar, M. S., Gilani, Z. A., & Asgar, H. M. N. ul H. K. (2020). Impact of aluminum substitution on the structural and dielectric properties of Ni–Cu spinel ferrite nanoparticles synthesized via sol–gel route. *Opt. Quantum Electron* , 52(4), 1–17. https://doi.org/10.1007/s11082-020-02304-w

Batoo, K. M., Kumar, S., Lee, C. G., & Alimuddin. (2009). Finite size effect and influence of temperature on electrical properties of nanocrystalline Ni-Cd ferrites. *Curr. Appl. Phys.*, 9(5), 1072–1078. https://doi.org/10.1016/j.cap.2008.12.002

Mahmood, M. F., & Hossen, M. B. (2021). Dynamic response of electrical, dielectric and magnetic properties of La-substituted Ni-Cu-Cd bulk ceramics with structural rietveld refinement. *J. Mater. Sci.: Mater.*, 32(11), 14248–14273. https://doi.org/10.1007/s10854-021-05988-2

Şaşmaz Kuru, T., Eyüpoğlu, V., & Yıldız, F. (2018). The effect of Al^{3+} additive on the structural, optical, and magnetic properties of Al–Cd ferrites fabricated by coprecipitation method. *In Acta Physica Polonica A* 134, 1092. https://doi.org/10.12693/APhysPolA.134.1092

Batoo, K. M. (2011). Microstructural and Mössbauer properties of low temperature synthesized Ni-Cd-Al ferrite nanoparticles. Nanoscale Res. Lett., 6, 1. https://doi.org/10.1186/1556-276X-6-499

Sapna, Budhiraja, N., Kumar, V., & Singh, S. K. (2018). X-ray Analysis of NiFe 2 O 4 Nanoparticles by Williamson-Hall and Size-Strain Plot Method . *J. Adv. Phys*., 6(4), 492–495. https://doi.org/10.1166/jap.2017.1363

Ponpandian, N., & Narayanasamy, A. (2002). Influence of grain size and structural changes on the electrical properties of nanocrystalline zinc ferrite. *J. Adv. Phys.*, 92(5), 2770. https://doi.org/10.1063/1.1498883

Zak A.K, Esmaeilzadeh J. Hashim A.M. (2024). X-ray peak broadening and strain-driven preferred orientations of pure and Al-doped ZnO nanoparticles prepared by a green gelatin-based sol-gel method, *J. Mol. Struct.* 1303, 137537

F. Alam, M. L. Rahman, M. H. R. Khan, A. K. M. A. Hossain, (2014). Magnetic Hysteresis and Complex Initial Permeability of Cr^{3+} Substituted Mn-Zn Ferrites. *J. Mod. Phys.,* 05(14), 1223. https://doi.org/10.4236/jmp.2014.514122.

Birajdar, A. A., Shirsath, S. E., Kadam, R. H., Mane, M. L., Mane, D. R., & Shitre, A. R. (2012). Permeability and magnetic properties of Al^{3+} substituted $Ni_{0.7}Zn_{0.3}Fe_2O_4$ nanoparticles. *J.Appl. Phys.*, 112, 053908. https://doi.org/10.1063/1.4748959.

Zakaria, A., Hakim, M., & Asgar, M. (2009). Effect of Substitution of Al for Fe on the Magnetic Phase Transition and Initial Permeability of Zn-Co Ferrites. *J. Bang. Acad. Sci.*, 32(2). https://doi.org/10.3329/jbas.v32i2.2426

Massoudi, J., Smari, M., Nouri, K., Dhahri, E., Khirouni, K., Bertaina, S., Bessais, L., & Hlil, E. K. (2020). Magnetic and spectroscopic properties of Ni-Zn-Al ferrite spinel: From the nanoscale to microscale. *RSC Advances*, 10(57), 34556. https://doi.org/10.1039/d0ra05522k

Rahman, M. M., Hasan, N., Hoque, M. A., Hossen, M. B., & Arifuzzaman, M. (2022). Structural, dielectric, and electrical transport properties of Al3+ substituted nanocrystalline Ni-Cu spinel ferrites prepared through the sol–gel route. *Results in Phys.*, 38. https://doi.org/10.1016/j.rinp.2022.105610

Kulkarni, A. B., & Mathad, S. N. (2018). Synthesis and Structural Analysis of Co–Zn–Cd Ferrite by Williamson–Hall and Size–Strain Plot Methods. *Int. J. Self-Propagating High-Temp. Synth.* 27(1), 37–43. https://doi.org/10.3103/S106138621801003X

Shetty, P. B., Maddani, K. I., MahaLaxmi, K. S., Lakshmi, C. S., & Sridhar, C. S. L. N. (2023). Studies on lanthanum-doped nickel ferrites for improved structural, magnetic and optical properties, *J. Mater. Sci.: Mater.,* 34(15), 1–15. https://doi.org/10.1007/s10854-023-10542-3

Jogi, J. K., Singhal, S. K., Jangir, R., Dwivedi, A., Tanna, A. R., Singh, R., Gupta, M., & Sagdeo, P. R. (2022). Investigation of the Structural and Optical Properties of Zinc Ferrite Nanoparticles Synthesized via a Green Route. *J. Electron. Mater.*, 51(10), 5482–5491. https://doi.org/10.1007/s11664-022-09813-2

Sattar, A., Bofeng, B., Khalil, M., & Sajjad, M. (2022). Detailed analysis of structural, optical and photo catalytic properties of spinel nickel doped magnesium zinc ferrites at different substitutions. *Inorg. Chem.,* 142, 109505. https://doi.org/10.1016/j.inoche.2022.109505

Sharma, A., Batoo, K. M., Aldossary, O. M., Jindal, S., Aggarwal, N., & Kumar, G. (2021). Investigation of dielectric, electrical and optical properties of copper substituted Mn-Zn nanoferrites, *J. Mater. Sci.: Mater.*, 32(1), 313. https://doi.org/10.1007/s10854-020-04782-w

M. A. Ali, M. N. I. Khan, F. U. Z. Chowdhury, M. M. Hossain, A. K. M. A. Hossain, R. Rashid, , A. Nahar, S. M. Hoque, M. A. Matin, M. M. Uddin (2019), Yttrium-substituted Mg–Zn ferrites: correlation of physical properties with Yttrium content. *J. Mater. Sci.: Mater.* , 30(14), 13258. https://doi.org/10.1007/s10854-019-01689-z.

Islam, M. A., Rahaman, M. Z., Hasan, M. M., & Hossain, A. K. M. A. (2019). Analysis of grain growth, structural and magnetic properties of Li-Ni-Zn ferrite under the influence of sintering temperature. *Heliyon*, 5(2), e01199. https://doi.org/10.1016/j.heliyon.2019.e01199

Mostafa, M., Saleh, O., Henaish, A. M., El-Kaream, S. A. A., Ghazy, R., Hemeda, O. M., Dorgham, A. M., Al-Ghamdi, H., Almuqrin, A. H., Sayyed, M. I., Trukhanov, S. V., Trukhanova, E. L., Trukhanov, A. V., Zhou, D., & Darwish, M. A. (2022). Structure, Morphology and Electrical/Magnetic Properties of Ni-Mg Nano-Ferrites from a New Perspective. *Nanomater*., 12(7). https://doi.org/10.3390/nano12071045

Smit, J., & Win, H.M.J., (1959), FERRITES, Philips' Technical Library, Eindhoven, Netherlands 78.

Jelonek J. and Szczyciel M. (1978). Dispersion of Initial Magnetic Permeability for $HgCr_2Se_4$. *Phys. Stat. Sol.* 50, 679. https://doi.org/10.1002/pssa.2210500238

Nam, J.H., Jung, H.H., Shin, J.Y., & Oh, J.H (1995). The effect of Cu substitution on the electrical and magnetic properties of NiZn ferrites. *IEEE Trans. Magn*. 31, 3985. https://ieeexplore.ieee.org/document/489838/authors#authors